


ORIGINAL ARTICLE

# Time and cell-dependent effects of endocytosis inhibitors on the internalization of biomolecule markers and nanomaterials

Luana Sasso,<sup>1,2</sup> Laura Purdie,<sup>1,2</sup> Anna Grabowska,<sup>2</sup> Arwyn Tomos Jones<sup>3</sup> & Cameron Alexander<sup>1\*</sup> 

<sup>1</sup> School of Pharmacy, University of Nottingham, Nottingham NG7 2RD, UK

<sup>2</sup> School of Medicine, University of Nottingham, Nottingham NG7 2RD, UK

<sup>3</sup> School of Pharmacy and Pharmaceutical Science, Cardiff University, Cardiff, Wales CF10 3NB, UK

## Keywords

Endocytosis, intracellular trafficking, chlorpromazine, methyl- $\beta$ -cyclodextrin, nanoparticles, nanomedicines.

## Corresponding Author:

Cameron Alexander, School of Pharmacy,  
University of Nottingham, NG7 2RD, UK.  
Tel: +44 (0)115 846 7678  
Email: cameron.alexander@nottingham.ac.uk.

## FUNDING INFORMATION

Engineering and Physical Sciences Research Council (EP/H005625/1EP/J021180/1EP/N03371X/1, EP/N03371X/1, EP/J021180/1, EP/H005625/1); Office of the Royal Society (WM150086)

Received: 04 April 2018;

Revised: 19 April 2018;

Accepted: 30 April 2018

Journal of Interdisciplinary  
Nanomedicine,  
2018; 3(2), doi: 10.1002/jin2.39

## Abstract

Endocytosis is an essential function of cells, with key roles in the internalisation of nutrients, signal molecules and also drugs. Endocytic processes are therefore widely investigated in the context of drug delivery, and inhibitors of endocytic pathways have been used to provide information regarding uptake mechanisms of drug carrier materials. Here we describe studies in which two established inhibitors of clathrin dependent and independent endocytosis, chlorpromazine and methyl- $\beta$ -cyclodextrin respectively, were employed to probe endocytic pathways of three cell lines chosen to represent tumour-relevant or associated phenotypes: 3 T3 (fibroblasts), HCT 116 (colon cancer) and MGLVA-1 (gastric cancer). For clathrin mediated endocytosis the data highlight that chlorpromazine inhibition of transferrin internalization, via clathrin dependent endocytosis, is cell and time dependent. We also show that inhibition of uptake is transient with a resumption of transferrin internalization after a maximal inhibition period. The same endocytosis inhibitors were used to probe the internalization of 50 and 100 nm carboxylated polystyrene nanoparticles (C-PS-NPs) as model drug delivery carriers. Flow cytometry data indicated that internalisation of C-PS-NPs varied considerably with the incubation time of cells with chlorpromazine or methyl- $\beta$ -cyclodextrin, and that the effects were also markedly cell-line dependent. These data highlight that the effects of endocytosis inhibitors on the internalisation pathways even of relatively simple nanoparticles are complex and interdependent. We suggest that mechanistic investigations of the endocytic processes which govern practical applications of nanoparticles for diagnostic and therapeutic applications should be considered on a cell, time and concentration basis.

## Introduction

In recent years, drug delivery systems have moved beyond the investigational stage to the extent that many have now reached the market. (Peppas, 2013) Furthermore, progress in synthetic chemistry has widened the field of new delivery materials such that highly-defined systems can now be programmed to effect drug release in response to disease-specific environmental changes. (Koyamatsu et al., 2014; Zan et al., 2015) These materials may form a new class of 'nanomedicines' delivering and releasing drugs through patient- or disease-related changes at the cellular and subcellular level. (Bremer-Hoffmann et al., 2018; Chan et al., 2014; Khan et al., 2014) However, in order to convert more of the new carrier systems from the investigational to the clinical phase, much greater understanding of the mechanisms that cells use to process nanomaterials is needed. (Li et al., 2017)

Prior reports have shown that the entry of nanomaterials into cells, their subsequent trafficking and fate takes place via multiple, complex and sometimes overlapping endocytic routes. (Chierico et al., 2014; Donnellan et al., 2017; Fowler et al., 2013a; Lu et al., 2015; Moody et al., 2015; Tekle et al., 2008) The study of novel nanoparticles intended for drug delivery requires that these cell mechanisms are probed for uptake efficiency, pathway and kinetics. (Iversen et al., 2011; Johnston et al., 2010) To date, the standard experiments have involved the screening of cells with drug delivery nanoparticles (NPs) in the presence of endocytosis inhibitors to assess the pathways of NP internalization and trafficking. (Li et al., 2015; Liu et al., 2015; Quan et al., 2015) Typical inhibitor studies involve their addition to cell culture media followed by addition of labelled NPs for short periods of 1-2 hrs before obtaining a readout from, most often, flow cytometry or microscopy.

Here, in the specific context of nanoparticle delivery, we evaluate the use of chlorpromazine (CPZ), an established inhibitor of clathrin mediated endocytosis (CME), and methyl- $\beta$ -cyclodextrin (M $\beta$ CD), which extracts cholesterol from the membrane of cells and thus inhibits clathrin independent pathways (CIE), including those which take place via caveolae. We aimed to establish the activities of these inhibitors in cell lines of relevance to cancer therapy, and across time and concentration ranges which might be utilised in drug delivery experiments. The iron-transport protein human transferrin (HTf) and the lipid lactosylceramide (LacCer) were employed as markers of CME and CIE,

respectively. (Vercauteren et al., 2010) These two inhibitors were tested in 3 T3 fibroblasts, epithelial HCT 116 colon cancer and MGLVA-1 gastric cancer cells to cover the intended range of potential biological targets. Carboxylated polystyrene nanoparticles (C-PS-NPs) of 50 and 100 nm were chosen as simple, readily available models of drug delivery carriers and their internalization was probed in these three cell lines treated with the inhibitors at different incubation times.

In this paper we show that the inhibition of endocytosis of HTf with CPZ is markedly cell- and time- dependent. In addition, the extent of inhibition is highly dependent on the concentration of CPZ used and the same is true for HTf internalization after inhibition. The data further indicate that the actions of CPZ and M $\beta$ CD, which are widely used in drug delivery and cell biology experiments, are more elaborate than commonly reported and that experimental protocols using these inhibitors need to be adapted specifically for the particular cell and carrier systems under investigation. Given the reported concerns on the low success rates for translating lab-based nanomedicines to the clinic, we believe the experiments reported here can help in the search for standardised and readily transferable studies of drug delivery nanoparticles *in vitro*.

## Materials and methods

The gastric cancer cells were derived from the MGLVA-1 line -as ascites of a variant of MKN45 human gastric adenocarcinoma cells and were cultured according to procedures developed in our laboratories. (Watson et al., 1990) Other cell lines including HCT 116 human colon cancer cells (Brattain et al., 1981), and 3 T3-Swiss albino mouse embryo fibroblasts were purchased from the American Type Culture Collection (ATCC) and LGC Standards, Teddington, UK. All cells were cultured and recovered in Roswell Park Memorial Institute (RPMI) medium or Dulbecco Modified Eagle Medium (DMEM) supplemented with 10% v/v heat inactivated Foetal Bovine Serum (FBS) and 2 mM L-glutamine (Sigma-Aldrich, Dorset, UK) according to specifications from the ATCC and Cell Bank.

The dyes BODIPY FL C5-lactosylceramide, (LacCer) complexed to BSA,<sup>‡</sup> and Cell Mask deep red plasma membrane stain were purchased from Molecular Probes

<sup>‡</sup>BODIPY-labeled LacCer was applied to the cells as a complex with BSA, which makes the lipid marker water-soluble and therefore more easily presented to cell surfaces.

(Paisley, UK). A specific defatted albumin preparation (dBSA), the inhibitors chlorpromazine (CPZ), methyl- $\beta$ -cyclodextrin (M $\beta$ CD) and the buffer 2-[4-(2-hydroxyethyl)piperazin-1-yl] ethanesulfonic acid (HEPES) were obtained from Fisher Scientific, Loughborough, UK.

Carboxylated polystyrene nanoparticles (C-PS-NPs) with diameters of 50 nm (catalogue number 19775) and 100 nm diameter (catalogue number 18791),  $\lambda_{\text{max}}$  ex 529 nm -  $\lambda_{\text{ma}}$ x em 546 nm, were purchased as Polystyrene Fluoresbrite Yellow-Orange particles from Polysciences, Heppenheim, Germany. These polystyrene particles were similar in zeta potentials, with values of  $-37.7$  mV for the 50 nm nanoparticles and  $-34.2$  mV for the 100 nm NPs.

### Flow cytometry

Cells were seeded for flow cytometry studies in 25cm<sup>2</sup> vented cap flasks at a concentration of 31200 cells/cm<sup>2</sup> and allowed to attach to the bottom of the flasks overnight. In the next step, HBSS medium, supplemented with 20 mM HEPES containing the appropriate endocytic pathway inhibitors, or 20 mM HEPES without inhibitors, was used to replace the full media and incubated with the cells for 30 mins. After this time, the solution was replaced with HBSS/HEPES 20 mM with or without lactosylceramide 0.81  $\mu$ M, human transferrin 6.7  $\mu$ g/ml, and the appropriate-sized (50 or 100 nm diameter) carboxylated polystyrene nanoparticles (C-PS-NPs). When the experimental assay time was complete, the cells were washed again, detached from the flasks with trypsin-EDTA or EDTA alone, centrifuged at 2000 g for 5 mins and re-suspended in PFA 4% v/v in PBS as a fixation buffer. An acidic cell wash was used to remove HTf which had remained membrane-bound after the initial washes: this consisted of Hank's Minimum Essential Medium devoid of glucose +0.1% w/v NaN<sub>3</sub> (HMEM-G) + I (2 times at 4 °C) followed by an ice cold wash for 1 min with 0.2 mM acetic acid 0.2 mM NaCl buffer. A residual acidic solution was removed by 2 further washes with cold HMEM-G + I. Removal of excess LacCer was via two ice cold washes with HMEM-G + I followed by 6 rinse steps (10 mins each) of HMEM-G + I supplemented with 5%w/v dBSA (back exchange method). A BD LSR II flow cytometer with an APC 660/20 bandpass filter for HTf and FITC 530/30 bandpass filter for LacCer was used to quantify fluorescence in the cells resulting from endocytosed nanoparticles.

### Effects of C-PS-NPs, CPZ and M $\beta$ CD on cells via Cell Titer Glo assays

Cells were seeded at a density of 31200 cells/cm<sup>2</sup> in the middle 60 wells of a clear-bottom, black-sided 96 well plate and allowed to attach to the bottom of the wells overnight. After checking for cell attachment, the media were aspirated and replaced with 100  $\mu$ l of the test solution/suspension in HBSS/HEPES 20 mM in triplicates. Three independent experiments were carried out. For the nanoparticle uptake assays, C-PS-NPs of 50 and 100 nm were tested at concentrations of 100  $\mu$ g/ml for 4 h. The endocytic pathway inhibitors CPZ and M $\beta$ CD were tested at 80  $\mu$ M and 1.25 mM respectively for 4.5 h. For each experiment a positive control (PEI 0.5 mg/ml) and negative control (HBSS/HEPES 20 mM) were also used. As a blank control, the fluorescence of HBSS/HEPES 20 mM without cells was recorded under the same conditions. Cell suspensions containing C-PS-NPs were incubated at 37 °C in a 5% CO<sub>2</sub> atmosphere for 4 h. Endocytosis inhibitors were incubated with cells for 4.5 h. At a time point of 15 minutes before the experimental incubation period for cells and particles/inhibitors was complete, the cells were removed from the incubator and left to equilibrate to room temperature. Subsequently, a solution of Cell Titer Glo mix (100  $\mu$ l) was applied and the 96 well plates were loaded on an orbital mixer for 2 minutes to allow sufficient time for cell lysis. The plate was further incubated at room temperature for 10 minutes to ensure a stable luminescence signal. In experiments with the C-PS-NPs, the supernatants in each well were removed with a pipette tip, and 100  $\mu$ l of HBSS/HEPES 20 mM applied, prior to the application of the Cell Titer Glo mix. This extra step was required to reduce possible interactions of the Cell Titer Glo enzyme with extracellular nanoparticles. The luminescence recorded for 1 second per well according to the manufacturer's specifications on a FluoStar Optima microplate reader (BMG LABTECH GmbH, Ortenberg, Germany).

### Live cell imaging of C-PS-NPs in 3 T3, HCT 116 and MGLVA-1 cells via confocal microscopy

For the imaging experiments, pre-sterilised rounded 22x1.5 mm glass coverslips were placed in 6 well plates in full media. Cells at a density of 31200 cells/cm<sup>2</sup> were added to the wells and allowed to attach to the glass coverslips overnight. When attachment was confirmed, the cells were stained with Hoechst 33342 (Thermo Scientific, Rockford, USA and CellMask deep red

(Molecular Probes, Paisley, UK) cell membrane stain (both stains at a concentration of 1  $\mu\text{g}/\text{ml}$ ) for 30 minutes. The media was then replaced with HBSS/HEPES 20 mM for live imaging. The microscope used for the imaging was a Zeiss Laser Scanning Microscope (LSM) 710, (Jena, Germany) equipped with a heated chamber and holders for samples (in this case coverslips) pre-warmed to 37 °C. Microscopy images of dye-labelled cells in buffer were taken prior to the incubation assay of cells with the test C-PS-NPS. The polymer nanoparticle suspensions were added to the buffer solution at a 1:1 ratio to obtain a final concentration of C-PS-NPs of 50  $\mu\text{g}/\text{ml}$ . In order to cover representative numbers of cells in the images, at least 4 regions of interest for each assay were acquired, at timepoints of 10, 20, 30 and 60 minutes using the 40x objective lens of the confocal microscope.

## Statistics

Two way Anova statistical analysis was carried out with GraphPad Prism 6 and Bonferroni post-analysis tests.

## Results

To establish the optimal protocol for inhibiting endocytosis with CPZ or M $\beta$ CD we first identified conditions for maximal CPZ inhibition of HTf internalisation in terms of concentration and time of incubation in 3 T3, HCT 116 and MGLVA-1 cells. For this reason, 80  $\mu\text{M}$  of CPZ was applied for 1, 2, 3 and 4 h together with HTf after an initial HTf free 30 min preincubation. Here, the concentrations of the inhibitors were chosen as the highest which inhibited HTf uptake without inducing toxicity (Fig. S1). Initial experiments indicated that the effects of CPZ on the endocytosis of HTf and LacSer were temporary and occurred over an incubation time that was

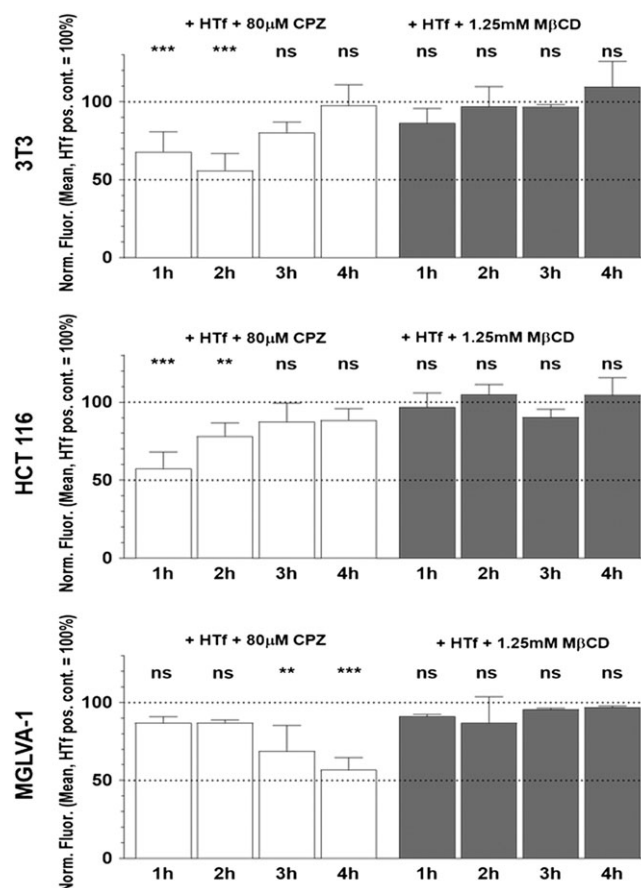


**Figure 1.** Time and cell dependence of HTf uptake inhibition by CPZ or M $\beta$ CD in 3 T3, HCT 116 and MGLVA-1 cells as determined by flow cytometry. Data shown are the combination of 2-6 independent experiments: mean and standard deviation of fluorescence for 10000-20000 gated cells shown for each experiment. Fluorescence was normalised against the HTf treated positive control for each period of internalisation (considered as 100% uptake). The dotted lines refer to 50 and 100% uptake of HTf. Statistical treatments: Two-Way ANOVA using an equation for samples of different sizes and Bonferroni post-analysis (\*  $P < 0.05$ ; \*\*  $P < 0.01$ ; \*\*\*  $P < 0.001$ ).

cell-dependent (Fig. 1). HTf uptake was inhibited to the greatest extent with CPZ at 1 and 2 h timepoints for 3 T3 fibroblasts, but at 1 h for HCT 116 cells and 4 h for MGLVA-1. Endocytosis of HTf returned to the same levels as occurred in the absence of inhibitors after 4 h in 3 T3 and HCT 116 cells.

Furthermore, as expected, inhibition of HTf by CPZ was concentration-dependent (Fig. 2) and again, after a period of maximal inhibition, HTf uptake in 3 T3 and HCT 116 cells was restored to the same levels as occurred in the absence of inhibitors. This suggested no gross toxicity of the inhibitors in these assays but the higher concentrations of CPZ used in these studies did increase cell recovery times as determined by HTf internalisation. M $\beta$ CD did not inhibit the internalization of HTf at any of the timepoints chosen in these studies.

To probe further the internalization mechanisms of HTf after CPZ treatment, inhibition studies with HBSS without Ca<sup>2+</sup> and Mg<sup>2+</sup> were carried out in 3 T3 fibroblasts. In these conditions cells should become energy-depleted, and thus less able to transport proteins into cells by active energy-dependent pathways. (Tarasov et al., 2012) Furthermore, the binding of ligands to membrane receptors and particularly the

binding of transferrin to its cognate transferrin receptors, is known to be inhibited by depletion of extracellular Ca<sup>2+</sup> (Andersen and Moestrup, 2014) The data in Figure 3 indicate that depletion of essential ions in these assays did not result in internalization of HTf to the same level as occurred in cells under the initial inhibitor-free conditions (Fig. 1). In turn, this suggested that the restoration of HTf uptake is an energy dependent process which does not occur in energy-depleted and stressed cells. Once again no significant effects on HTf uptake were noted in these fibroblasts incubated with M $\beta$ CD.

Subsequently, the effect of higher passage number following the splitting of cells was studied and the extent of endocytosis inhibition was investigated in 3 T3 and HCT 116. Endocytic uptake of HTf was reduced at passage numbers ranging between 28 and 53 in 3 T3 fibroblasts and at passage numbers 18-44 in HCT 116. As apparent from figure 4, CPZ was able to inhibit uptake of HTf but this effect was diminished at higher cell passage numbers. In addition, the difference between inhibited and uninhibited cells was reduced and there was found to be no statistical significance between control and CPZ treated cells after 3 h for the higher passage 3 T3, and at all timepoints in HCT 116 cells.

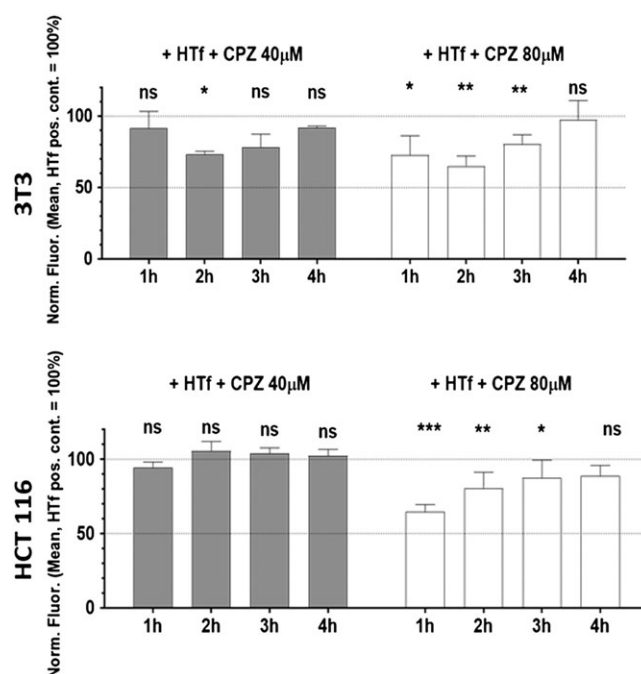


**Figure 2.** Concentration and time dependence of HTf uptake inhibition by CPZ in 3 T3 and HCT 116 cells. Flow cytometry data normalised against fluorescence of HTf positive control and expressed at the mean and standard deviation of a minimum of 10000 gated cells for each experiment ( $n = 2$ ). The dotted lines refer to 50 and 100% uptake of HTf. Statistical treatments: Two-Way ANOVA and Bonferroni post-analysis tests for significant differences (\*  $P < 0.05$ ; \*\*  $P < 0.01$ ; \*\*\*  $P < 0.001$ ).



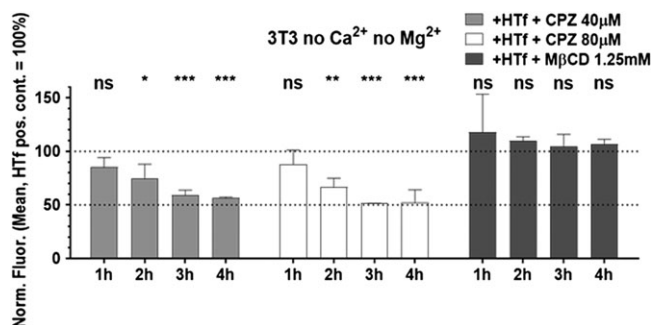


**Figure 3.** Effects of Ca<sup>2+</sup> and Mg<sup>2+</sup> depletion on the uptake of HTf with CPZ in 3 T3 cells. Results shown are represented as the mean and standard deviation of 2 independent experiments, normalised against the HTf positive control and show the mean and the standard deviation of 10000 gated cells. The dotted lines refer to 50% and 100% uptake of HTf. Error bars represent the standard deviation of the mean of duplicate experiments,  $n = 2$ . Statistical treatments: Two-Way ANOVA and Bonferroni post-analysis test for significant differences (\*  $P < 0.05$ ; \*\*  $P < 0.01$ ).

MβCD depletes cholesterol from plasma membranes and previous studies have shown that uptake of the lipid LacCer is inhibited in cells treated with this compound. (Vercauteren et al., 2010) Data in Figure 5 confirm this, showing significant inhibition of uptake in the three cell lines tested, with 3 T3 cells being the most responsive. In contrast to CPZ, the reduction of LacCer uptake with MβCD was less dependent on cell-passage and time. A one hour incubation period with the drug and lipid, following a 30 min preincubation period, resulted in the greatest reduction of endocytosis in 3 T3 cells, whereas at least 2 h incubation was necessary for HCT 116 and MGLVA-1 cells. When CPZ was used as a control inhibitor for clathrin-independent endocytosis, a substantially increased uptake of LacCer was apparent in all cells tested. In Figure 5 the data indicate that endocytosis of LacCer occurred to levels approximately 3 fold higher than those observed in the positive control.

In the subsequent functional assays, carboxylated polystyrene nanoparticles (C-PS-NPs) of 50 and 100 nm nominal diameter were chosen as easily accessible models of drug delivery carriers. Nanoparticles based on polystyrene have been extensively studied in many cell lines with and without attached targeting ligands for their effects on viability and apoptosis, and also in terms of their internalization pathways. (Fowler et al., 2013a; Fowler et al., 2013b; Milani et al., 2012; Varela et al., 2012) The polystyrene nanoparticles were also similar in zeta potentials, with values of  $-37.7$  mV for the 50 nm nanoparticles and  $-34.2$  mV for the 100 nm NPs, and thus were expected to be colloidally stable but not to vary in uptake via a charge-dependent mechanism.

Initial assays indicated that both types of carboxylated polystyrene nanoparticles (50 and 100 nm diameter) were rapidly internalised by all 3 cell lines (Fig. 6). Higher magnification images (Fig. 7) indicated only minor variation in the intracellular location of nanoparticles in the three cell lines, and nor were there any clear differences between distribution of 50 nm vs 100 nm C-PS-NPs at either 30 minutes or 60 minutes. However, there were some apparent differences in sizes of punctate regions of fluorescence across the cell lines and particle size ranges over the two time periods, potentially indicative of changes in trafficking pathways of the nanoparticles following internalisation (Fig. 7). In HCT116 cells the 50 nm C-PS-NPs at both time points were localised to a tight juxtanuclear region, but 100 nm particles showed a wider distribution profile surrounding the nucleus.

The kinetics of uptake and internalization pathways for the C-PS-NPs were therefore studied in the absence and presence of CPZ and MβCD at time periods of 1 hr and above (Fig. 8), as the initial experiments (Figs. 6 and 7) had suggested that maximal endocytic uptake was rapidly reached (1 hr) in all cases.

However, because the inhibition of CME with CPZ occurred at 4 h incubation in MGLVA-1 cells, we also evaluated uptake at a 4 h time point for this cell line. There were wide variations in uptake of C-PS-NPs across the cell lines when inhibitors were added compared to the uptake in the absence of inhibitors, but statistically significant inhibition of internalization was only obtained with 50 nm C-PS-NPs at 1 and 2 h in HCT 116 cells. This is overall in good agreement with the times found for inhibition of the endocytic markers HTf and LacCer. Intriguingly, CPZ significantly increased uptake of 100 nm

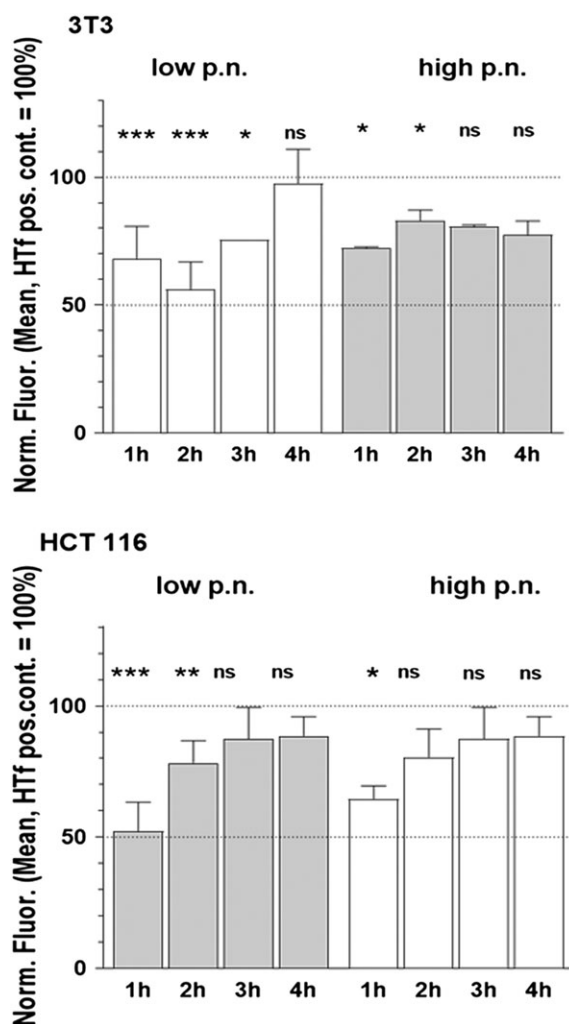


**Figure 4.** Passage number and ageing of cells affects HTf uptake in the presence of CPZ (80  $\mu$ M). Graphs show inhibition with 80  $\mu$ M CPZ in 3 T3 and HCT 116 cells with more than 20 passage numbers difference. Data represent three replicate data points for each experiment for a minimum 2 independent experiments. Mean and standard deviation of a minimum of two independent experiments (10000 gated cells for each experiment) are shown. Statistical treatment: Two-Way ANOVA using an equation for samples of different sizes and Bonferroni post-analysis tests for significant differences (\*  $P < 0.05$ ; \*\*  $P < 0.01$ ; \*\*\*  $P < 0.001$ ).

C-PS-NPs at 1 hr in HCT-116 cells compared to the same experiments without CPZ. In contrast, M $\beta$ CD did not inhibit uptake of either size of C-PS-NPs in any cell line, and apparent increases in uptake for the 100 nm C-PS-NPs were not statistically significant.

## Discussion

In this study, we aimed our initial experiments on clathrin-mediated endocytosis (CME) to focus on chlorpromazine (CPZ), as a representative CME inhibitor.

CPZ is a dopamine antagonist and has an amphiphilic structure enabling intercalation in the inner leaflet of cell membranes.(Ferrell Jr. et al., 1988) Its cationic portion interacts with the negative charge of phospholipids and, in particular, phosphoinositides.(Chen et al., 2003) CPZ has been reported to inhibit endocytosis by binding to calmodulin, which regulates the recruitment of the myristoylated alanine-rich C-kinase substrate protein (MARCKS), which in turn acts to sequester the phospholipid phosphatidylinositol 4,5-bisphosphate (PI(4,5)P<sub>2</sub>). (Marshak et al., 1985) The process of CME requires the phospholipid in the binding of the AP-2 adaptor protein with the plasma membrane.(Eisenberg et al., 2008; Levin and Weiss, 1976) Accordingly, when CPZ binds to calmodulin, the cascade of protein and lipid recognition is disrupted and clathrin-mediated uptake is reduced. The variations in the inhibition times of CPZ in the different cell lines might therefore be expected to be due to the extent of CME activity in the cells, and accordingly the overall levels of clathrin available. Differential increases in MARCKS expression might also be expected to inhibit HTf uptake more rapidly, and different cell lines have been shown to express notably varied levels of MARCKS.(Rose et al., 1994) However, prior studies by Bickeboller *et al.* (Bickeboller et al., 2015; Rose et al., 1994) have shown that HCT 116 cells express only moderate levels of MARCKS, yet this cell line displayed the quickest response to inhibition by CPZ in our studies. Different levels of calmodulin in the various cell lines before or after exposure to CPZ or a calmodulin-like function exploited by other proteins expressed in immortalised and cancerous cells may also have contributed to the time-dependence of HTf uptake. (Kaneno et al., 2011) Thus while it was not altogether surprising to observe a time-dependency of HTf uptake inhibition, as cells inevitably will respond to the presence of a specific modulation in enzyme activity, the finding that CPZ activity and the time-dependence of HTf uptake varied so markedly across the 3 cell lines was not expected.

We then evaluated the possibility that the time dependency of CPZ inhibition was due to the action of efflux pumps pumping out CPZ in response to CPZ perturbation of cellular functions. Indeed, the expression levels of efflux pumps on the plasma membrane of cancer cells are often upregulated.(Mazard et al., 2013) However, CPZ is known to inhibit efflux pumps in addition to binding to calmodulin.(Amaral et al., 2010; Amaral et al., 2012; Ford et al., 1989; Ford

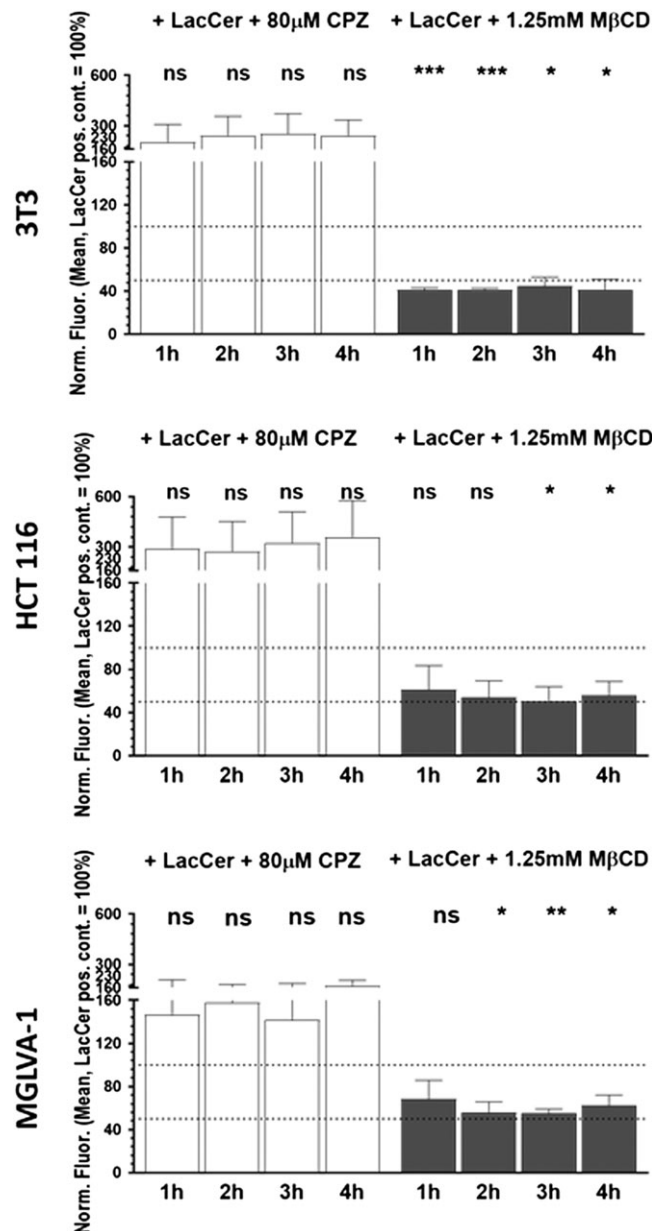


**Figure 5.** Respective inhibition and stimulation of LacCer uptake by MβCD and CPZ. A pre-incubation step of 30 min was carried out in the presence or absence of endocytosis inhibitors. Cells were incubated for up to 4 h and the results are the combination of 2 independent experiments (n = 2), the error bars represent the standard deviation of the mean from a minimum of 20000 gated cells per experiment. The dotted lines refer to 50 and 100% uptake of LacCer. Statistical treatment; T-test of CPZ or MβCD treated cells against untreated controls shows statistical significance. (ns: non significant,  $P > 0.05$ ; \*:  $P < 0.05$ ; \*\*:  $P < 0.01$ ; \*\*\*:  $P < 0.001$ ).

et al., 1990; Nacs et al., 1998) We therefore inferred that the mechanism by which HTf endocytosis returned to normal levels was due to the physicochemical properties of CPZ at membranes. CPZ has been reported to be a pore-forming molecule and has been used as a promoter of membrane fusion in experiments studying the dynamics of membrane reorganization in cells. (Kozlovsky et al., 2002) However, it should be noted that CPZ has been demonstrated to exhibit

membrane-fusion properties only at concentrations near to its critical micelle concentration (4 mM), (Mondal Roy and Sarkar, 2011) i.e. well above the concentrations used in our studies (which were  $\leq 80 \mu\text{M}$ ). Concentrations of CPZ above  $50 \mu\text{M}$  have been reported to produce leakage of low molecular weight cytoplasmic materials in platelets ( $< 2000 \text{ Da}$ ) suggesting that CPZ is able to produce small pores in the membrane of cells. (Holmsen and Rygh, 1990) Nevertheless, since



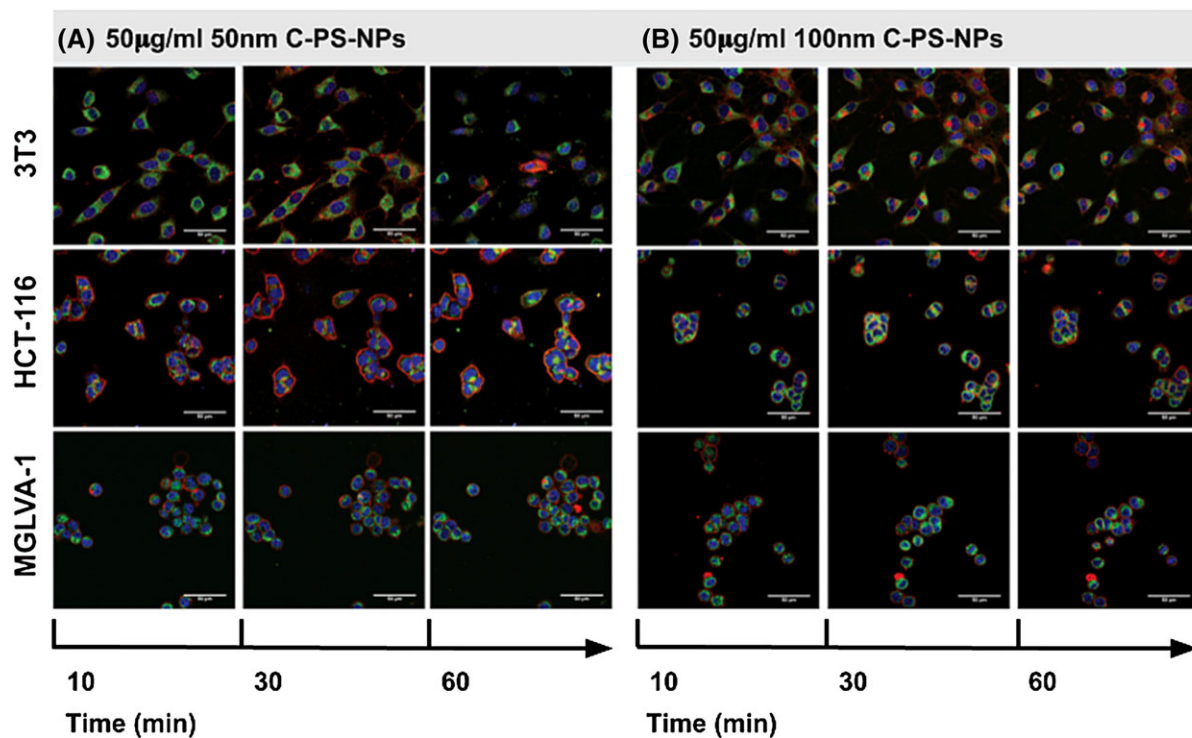


**Figure 6.** Live cell images of the uptake of (i) 50 nm and (ii) 100 nm C-PS-NPs in 3 T3, HCT 116 and MGLVA- 1 cells before the application of C-PS-NPs (time 0) and at, 10, 20, 30 and 60 min incubation with 50  $\mu\text{g}/\text{ml}$  C-PS-NPSC-PS-NPs in HPSS/Hepes buffer 20 mM. Scale bars represent 50  $\mu\text{m}$ . In the images the colours represent the following: Green = C-PS-NPs; Red = CellMask membrane staining; Blue = Nuclei (DAPI).

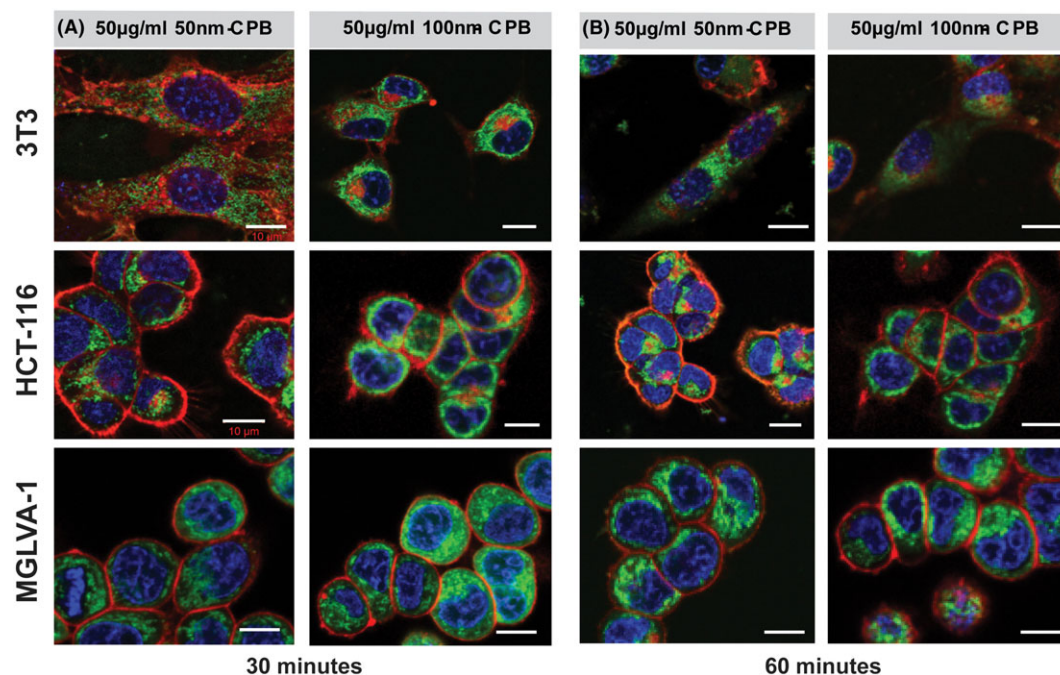


**Figure 7.** Comparison of cellular location of NPs at (i) 30 minutes and (ii) 60 minutes. Scale bars are 10  $\mu\text{m}$ . In the images the colours represent the following: Green = C-PS-NPs; Red = CellMask membrane staining; Blue = Nuclei (DAPI).

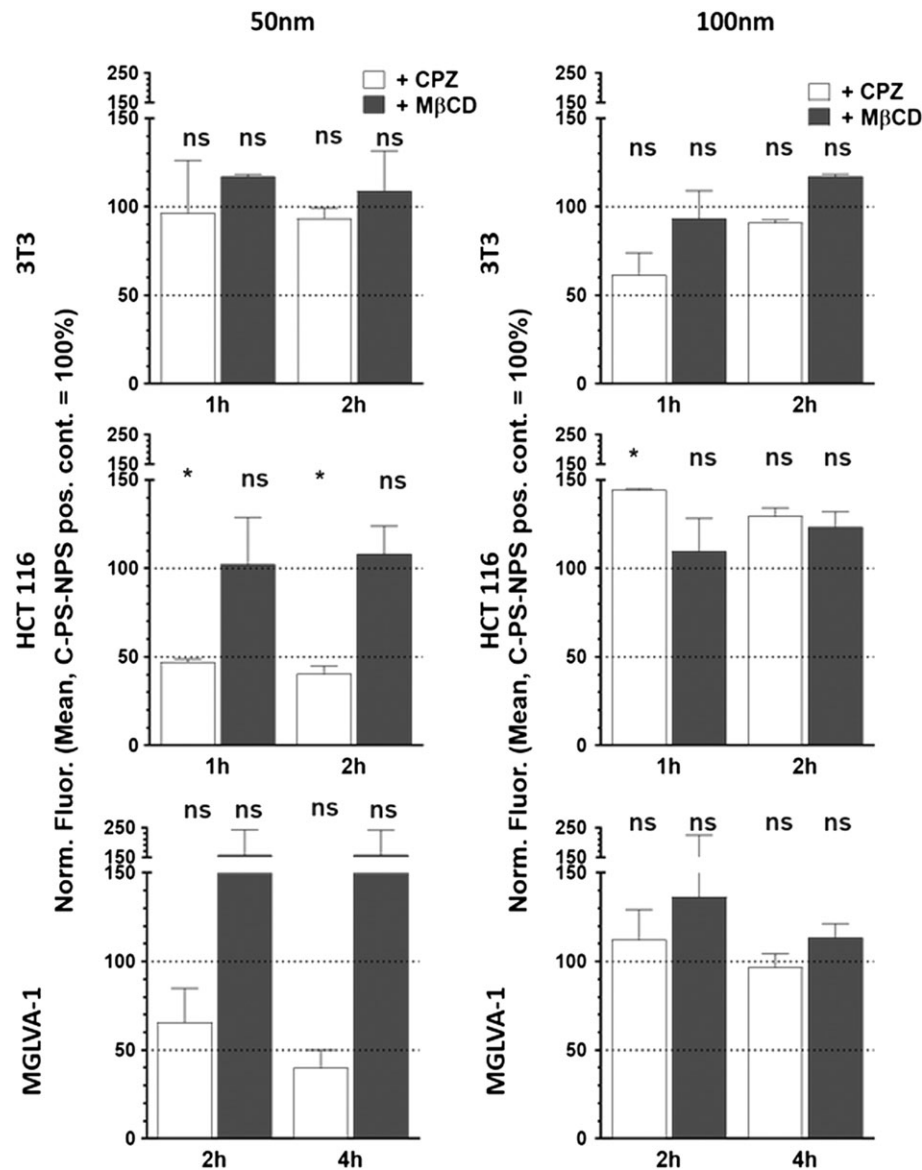


**Figure 8.** Endocytosis of 50 nm and 100 nm C-PS-NPs by cells with and without 80  $\mu$ M CPZ and 1.25 mM M $\beta$ CD. A pre-incubation step of 30 min was carried out in the presence or absence of endocytosis inhibitors. Cells were incubated for up to 4 h and the results are the combination of 2 independent experiments (n = 2). Uptake of C-PS-NPs in 3 T3 and HCT 116 cells was monitored for 1 and 2 h while in MGLVA-1 s uptake was examined at 2 and 4 h. The results are shown as the mean and standard deviation of 2 independent flow cytometry experiments obtained on 10000 gated cells (n = 2). The dotted lines refer to 50 and 100% uptake of C-PS-NPS. Statistical treatments: Two-Way ANOVA and Bonferroni post-analysis test for significant differences (ns: non significant; P > 0.05: \*)

HTf is a large and negatively charged protein (molar mass 80 kDa, pI ~ 5.8), it is unlikely incubation of cells with CPZ generated pores with sufficient size to allow passive transport of HTf. In addition, from the experiments using CPZ at 40 and 60  $\mu$ M, it was observed that HTf uptake after inhibition returned more readily to basal levels at lower concentrations, i.e. where any toxicity and pore-forming ability would be reduced. (Kilar and Simon, 1985) Further evidence that the observed HTf internalisation did not result from overt membrane damage was obtained from experiments

with 3 T3 cells in which media were used containing no Ca<sup>2+</sup> and Mg<sup>2+</sup>. In media without these two ions, the cells were expected to become energy-depleted, and thus less able to transport proteins into cells by active energy-dependent pathways. (Tarasov et al., 2012) The absence of Ca<sup>2+</sup> in extracellular media is also known to reduce the affinity of some membrane receptors to their ligands. (Andersen and Moestrup, 2014) As expected, in the absence of these ions, no recovery of HTf uptake was observed, with a reduction of HTf internalization over a period of 4 h in 3 T3 cells. Taken

together, these data suggest that CPZ caused a temporary interruption of active and energy-dependent transport processes which internalise HTf, as the subsequent recovery of HTf endocytosis was not indicative of a general toxicity or cell damage mechanism. Although there might be off target effects induced by CPZ, as it is a non-specific and complex inhibitor of endocytosis, the pattern of HTf uptake should be considered in the context of other possible transport mechanisms, such as internalization mediated via transferrin receptor 2 (TR2). (Bramini et al., 2014; Calzolari et al., 2006; Calzolari et al., 2007; Calzolari et al., 2009; Calzolari et al., 2010; Johnson et al., 2007)

In addition, the data on the inhibition of CME by CPZ showed the effects of different passage numbers of the cell lines used on the endocytosis of HTf. The finding that the higher the passage number or ageing of cells, the lower the levels of endocytosis inhibition by CPZ, may be attributed to the expression of dynamin, which is implicated in both clathrin and caveolin endocytosis. Levels of dynamin have been reported to be susceptible to passage number and confluence of cells. (Damke et al., 1995) The expression of calmodulin has also been shown to vary in relation to cell ageing and this might have been a further factor in the variation of HTf uptake with passage number. (Linskens et al., 1995) We ensured that the density of cells in these experiments was constant and at sub-confluent levels and thus it seems likely that the important determinant factor in HTf uptake was the passage number and ageing of cells, rather than confluence *per se*.

CPZ was also used in LacCer inhibition studies as a further control of CPZ specificity towards CME. Prior literature showed that CPZ did not inhibit the uptake of LacCer, (Ivanov, 2008) and our data were in accord with these findings. However, in our experiments, an increase in LacCer endocytosis was observed when CPZ was present, which agreed with results obtained by Vercauteren and coworkers. (Vercauteren et al., 2010) Time dependence of the enhancement of LacCer endocytosis with CPZ was apparent in 3 T3 and MGLVA-1 cells. No dependence on passage number of cells on the extent of the inhibition of LacCer uptake by CPZ was observed in these experiments (data not shown). In turn this indicates the inherent non specificity of CPZ towards caveolin and dynamin-mediated endocytosis in cases where passage number of cells is also a factor.

The experiments with the well-characterised protein HTf showed some unexpected results for inhibitor activity, so it is perhaps not surprising that extension of the

Inhibitor studies to the internalization of synthetic nanoparticles also yielded complex data. The effects of CPZ and M $\beta$ CD on the endocytosis of the C-PS-NPs were variable across both particle sizes and in the cell-lines studied. We originally chose the 50 and 100 nm C-PS NPs for our study since these are colloiddally stable materials with size ranges typical of nanoparticle diagnostics and delivery systems, and have been used before as model systems. (Bannunah et al., 2014; Byrne et al., 2015) Experiments with the negatively charged polystyrene nanoparticles by Bannunah *et al.* showed that the transport of 100 nm particles across Caco-2 and Calu-3 monolayers was suppressed by the dynamin-dependent endocytosis inhibitor dynasore, but that uptake was not affected. (Bannunah et al., 2014) These authors also showed that CPZ did not affect uptake of the negatively charged polystyrene nanoparticles, and while M $\beta$ CD reduced uptake and transport across Caco-2 and Calu-3 monolayers, this inhibitor had no effect on uptake in HeLa cells. (Bannunah et al., 2014) It is notable that the effects of CPZ on the internalisation of negatively-charged polystyrene in epithelial cells are similar to those that we observed for 100 nm C-PS-NPs in 3 T3 and MLGVA-1 cells, but at variance with the results we obtained for 50 nm C-PS-NPs in HCT-116 cells.

Taken together, our observations accord with those advocating that experimental conditions should be carefully established in the cell lines studied, and at incubation timepoints where the effects of the inhibitors are most clearly visible. (Rodal et al., 1999) The results shown here clearly highlight that nanoparticles can be internalised by different mechanisms in different cell lines and that the susceptibility to such inhibition depends on the cell line and the nature of the nanoparticle investigated. The data also highlights that in some cell types that NP uptake can be significantly increased by extraction of cholesterol from the plasma membrane. This could be further explored to identify whether this also leads to enhancing the overall performance of NPs when delivering small and macromolecular cargo to defined regions of a cell. It is also relevant to consider the uptake and transport processes for diagnostic nanoparticles, for example in those which bind to cell surface receptors and biomarkers. It has already been shown that multivalency of ligand-surface receptor interactions can alter both internalization pathways and intracellular fate of bioconjugates and nanoparticles, (Moody et al., 2015; Sayers et al., 2018) and thus for any diagnostic or sensing application the ultimate destination of a nanoparticle in one cell type may be rather

different in another cell type if the endocytic pathways are regulated differently. In addition, for therapeutic applications, it is clear that because there is variation in intracellular trafficking of simple nanoparticles even in relatively well-defined cell culture lines, one might expect even more variation in human patients. The fact that such marked differences are apparent in trafficking of nanoparticles between epithelial, fibroblastic and gastric and colon cancer cell variants suggests that in vivo application of therapeutic nanoparticles might require careful optimisation for individual patients also.

## Conclusions

These experiments show that the effect of commonly used chemical inhibitors on endocytosis such as CPZ and M $\beta$ CD are complex and their use should be tailored and optimised to the cell lines used for endocytosis studies. The study furthermore indicates that the effects of inhibitors on the internalization of endocytosis markers and of nanoparticles is cell, time and passage number dependent. Much of the recent literature on internalization of nanomaterials reports their route of uptake by extrapolating results from *in vitro* inhibition studies using chlorpromazine and other inhibitors of endocytosis. The results shown here suggest that some of the interpretation in the literature regarding internalization of nanomaterials in the presence of CPZ may need to be expanded to take into account cell- and time-dependency. In addition, the exact experimental protocols for inhibition studies with CPZ need to be evaluated carefully, and methods optimised for each specific cell line if detailed mechanistic insight into the endocytosis of synthetic nanomaterials is required.

## Acknowledgments

This work was supported by the Engineering and Physical Sciences Research Council grant numbers EP/H005625/1, EP/J021180/1, EP/N03371X/1); Office of the Royal Society (WM150086) and a Royal Society Wolfson Research Merit Award (WM150086) to CA. We also thank Matteo Weindelmayer, Tom Booth, Paul Cooling and Christine Grainger-Boulton for technical support.

Electronic Supplementary Information (ESI) available: [Cell Titer Glo toxicity tests of the working concentrations and experimental times of incubations used for 50 and 100 nm C-PS-NPS, CPZ and M $\beta$ CD, and further practical details for experiments in Figs. 1-5 and 8].

## Funding Information

EPSRC Grants EP/H005625/1, EP/J021180/1, EP/N03371X/1.

Royal Society Wolfson Research Merit Award (WM150086).

## REFERENCES

- Amaral, L., Martins, A., Molnar, J., Kristiansen, J. E., Martins, M., Viveiros, M., Rodrigues, L., Spengler, G., Couto, I., Ramos, J., Dastidar, S., Fanning, S., McCusker, M., and Pages, J. M. **2010**. Phenothiazines, bacterial efflux pumps and targeting the macrophage for enhanced killing of intracellular XDRTB. *In Vivo* 24:409-424.
- Amaral, L., Spengler, G., Martins, A., Armada, A., Handzik, J., Kiec-Kononowicz, K., and Molnar, J. **2012**. Inhibitors of bacterial efflux pumps that also inhibit efflux pumps of cancer cells. *Anticancer Res* 32:2947-2957.
- Andersen, C. B. F., and Moestrup, S. K. **2014**. How calcium makes endocytic receptors attractive. *Trends Biochem Sci* 39:82-90.
- Bannunah, A. M., Vllasaliu, D., Lord, J., and Stolnik, S. **2014**. Mechanisms of Nanoparticle Internalization and Transport Across an Intestinal Epithelial Cell Model: Effect of Size and Surface Charge. *Mol Pharm* 11:4363-4373.
- Bickeboller, M., Tagscherer, K. E., Kloor, M., Jansen, L., Chang-Claude, J., Brenner, H., Hoffmeister, M., Toth, C., Schirmacher, P., Roth, W., and Blaker, H. **2015**. Functional characterization of the tumor-suppressor MARCKS in colorectal cancer and its association with survival. *Oncogene* 34:1150-1159.
- Bramini, M., Ye, D., Hallerbach, A., Nic Raghnaill, M., Salvati, A., Åberg, C., and Dawson, K. A. **2014**. Imaging Approach to Mechanistic Study of Nanoparticle Interactions with the Blood-Brain Barrier. *ACS Nano* 8:4304-4312.
- Brattain, M. G., Fine, W. D., Khaled, F. M., Thompson, J., Thompson, D. E., Fau-Brattain, J., and Brattain, D. E. **1981**. Heterogeneity of malignant cells from a human colonic carcinoma. *Cancer Res* 41:1751-1756.
- Bremer-Hoffmann, S., Halamoda-Kenzaoui, B., and Borges, S. E. **2018**. Identification of regulatory needs for nanomedicines. *J Interdiscip Nanomed* 3:1-15.
- Byrne, G. D., Vllasaliu, D., Falcone, F. H., Somekh, M. G., and Stolnik, S. **2015**. Live Imaging of Cellular Internalization of Single Colloidal Particle by Combined Label-Free and Fluorescence Total Internal Reflection Microscopy. *Mol Pharm* 12:3862-3870.
- Calzolari, A., Deaglio, S., Maldi, E., Cassoni, P., Malavasi, F., and Testa, U. **2009**. TfR2 expression in human colon carcinomas. *Blood Cells Mol Dis* 43:243-249.
- Calzolari, A., Larocca, L. M., Deaglio, S., Finisguerra, V., Boe, A., Raggi, C., Ricci-Vitani, L., Pierconti, F., Malavasi, F., De Maria, R., Testa, U., and Pallini, R. **2010**. Transferrin Receptor 2 Is Frequently and Highly Expressed in Glioblastomas. *Trans Oncol* 3:123-134.
- Calzolari, A., Oliviero, I., Deaglio, S., Mariani, G., Biffoni, M., Sposi, N. M., Malavasi, F., Peschle, C., and Testa, U. **2007**. Transferrin receptor 2 is frequently expressed in human cancer cell lines. *Blood Cells Mol Dis* 39:82-91.
- Calzolari, A., Raggi, C., Deaglio, S., Sposi, N. M., Stafnes, M., Fecchi, K., Parolini, I., Malavasi, F., Peschle, C., Sargiacomo, M., and Testa, U. **2006**. TfR2 localizes in lipid raft domains and is released in exosomes to activate signal transduction along the MAPK pathway. *J Cell Sci* 119:4486-4498.
- Chan, N., An, S. Y., Yee, N., and Oh, J. K. **2014**. Dual Redox and Thermoresponsive Double Hydrophilic Block Copolymers with Tunable Thermoresponsive Properties and



- Self-Assembly Behavior. *Macromol Rapid Commun* 35:752-757.
- Chen, J. Y., Brunauer, L. S., Chu, F. C., Helsel, C. M., Gedde, M. M., and Huestis, W. H. **2003**. Selective amphipathic nature of chlorpromazine binding to plasma membrane bilayers. *Biochim Biophys Acta Biomembr* 1616:95-105.
- Chierico, L., Joseph, A. S., Lewis, A. L., and Battaglia, G. **2014**. Live cell imaging of membrane/cytoskeleton interactions and membrane topology. *Sci Rep* 4:6056.
- Damke, H., Baba, T., van der Bliek, A. M., and Schmid, S. L. **1995**. Clathrin-independent pinocytosis is induced in cells overexpressing a temperature-sensitive mutant of dynamin. *J Cell Biol* 131:69-80.
- Donnellan, S., Stone, V., Johnston, H., Giardiello, M., Owen, A., Rannard, S., Aljayyousi, G., Swift, B., Tran, L., Watkins, C., and Stevenson, K. **2017**. Intracellular delivery of nano-formulated antituberculosis drugs enhances bactericidal activity. *J Interdiscip Nanomed* 2:146-156.
- Eisenberg, S., Giehl, K., Henis, Y. I., and Ehrlich, M. **2008**. Differential Interference of Chlorpromazine with the Membrane Interactions of Oncogenic K-Ras and Its Effects on Cell Growth. *J Biol Chem* 283:27279-27288.
- Ferrell, J. E., Jr., Mitchell, K. T., and Huestis, W. H. **1988**. Membrane bilayer balance and platelet shape: morphological and biochemical responses to amphipathic compounds. *Biochim Biophys Acta* 939:223-237.
- Ford, J. M., Bruggemann, E. P., Pastan, I., Gottesman, M. M., and Hait, W. N. **1990**. Cellular and biochemical characterization of thioxanthenes for reversal of multidrug resistance in human and murine cell lines. *Cancer Res* 50:1748-1756.
- Ford, J. M., Prozialeck, W. C., and Hait, W. N. **1989**. Structural features determining activity of phenothiazines and related drugs for inhibition of cell growth and reversal of multidrug resistance. *Mol Pharmacol* 35:105-115.
- Fowler, R., Vllasaliu, D., Falcone, F. H., Garnett, M., Smith, B., Horsley, H., Alexander, C., and Stolnik, S. **2013b**. Uptake and transport of B12-conjugated nanoparticles in airway epithelium. *J Control Release* 172:374-381.
- Fowler, R., Vllasaliu, D., Trillo, F. F., Garnett, M., Alexander, C., Horsley, H., Smith, B., Whitcombe, I., Eaton, M., and Stolnik, S. **2013a**. Nanoparticle transport in epithelial cells: pathway switching through bioconjugation. *Small* 9:3282-3294.
- Holmsen, H., and Rygh, T. **1990**. Chlorpromazine makes the platelet plasma membrane permeable for low-molecular weight substances and reduces ATP production. *Biochem Pharmacol* 40:373-376.
- Ivanov, A. I. **2008**. Pharmacological Inhibition of Endocytic Pathways: Is It Specific Enough to Be Useful? *Methods Mol Biol* 440:15-36.
- Iversen, T. G., Skotland, T., and Sandvig, K. **2011**. Endocytosis and intracellular transport of nanoparticles: Present knowledge and need for future studies. *Nano Today* 6:176-185.
- Johnson, M. B., Chen, J., Murchison, N., Green, F. A., and Enns, C. A. **2007**. Transferrin Receptor 2: Evidence for Ligand-induced Stabilization and Redirection to a Recycling Pathway. *Mol Biol Cell* 18:743-754.
- Johnston, H. J., Semmler-Behnke, M., Brown, D. M., Kreyling, W., Tran, L., and Stone, V. **2010**. Evaluating the uptake and intracellular fate of polystyrene nanoparticles by primary and hepatocyte cell lines in vitro. *Toxicol Appl Pharmacol* 242:66-78.
- Kaneno, R., Shurin, G. V., Kaneno, F. M., Naiditch, H., Luo, J., and Shurin, M. R. **2011**. Chemotherapeutic agents in low noncytotoxic concentrations increase immunogenicity of human colon cancer cells. *Cell Oncol (Dordr)* 34:97-106.
- Khan, A. R., Magnusson, J. P., Watson, S., Grabowska, A. M., Wilkinson, R. W., Alexander, C., and Pritchard, D. **2014**. Camptothecin prodrug block copolymer micelles with high drug loading and target specificity. *Polym Chem* 5:5320-5329.
- Kilar, F., and Simon, I. **1985**. The effect of iron binding on the conformation of transferrin. A small angle x-ray scattering study. *Biophys J* 48:799-802.
- Koyamatsu, Y., Hirano, T., Kakizawa, Y., Okano, F., Takarada, T., and Maeda, M. **2014**. pH-responsive release of proteins from biocompatible and biodegradable reverse polymer micelles. *J Control Release* 173:89-95.
- Kozlovsky, Y., Chernomordik, L. V., and Kozlov, M. M. **2002**. Lipid Intermediates in Membrane Fusion: Formation, Structure, and Decay of Hemifusion Diaphragm. *Biophys J* 83:2634-2651.
- Levin, R. M., and Weiss, B. **1976**. Mechanism by which psychotropic drugs inhibit adenosine cyclic 3',5'-monophosphate phosphodiesterase of brain. *Mol Pharmacol* 12:581-589.
- Li, J., Mao, H., Kawazoe, N., and Chen, G. **2017**. Insight into the interactions between nanoparticles and cells. *Biomater Sci* 5:173-189.
- Li, Q., Liu, C.-G., and Yu, Y. **2015**. Separation of monodisperse alginate nanoparticles and effect of particle size on transport of vitamin E. *Carbohydr Polym* 124:274-279.
- Linskens, M. H., Feng, J., Andrews, W. H., Enlow, B. E., Saati, S. M., Tonkin, L. A., Funk, W. D., and Villeponteau, B. **1995**. Cataloging altered gene expression in young and senescent cells using enhanced differential display. *Nucleic Acids Res* 23:3244-3251.
- Liu, Y., Chen, Q., Xu, M., Guan, G., Hu, W., Liang, Y., Zhao, X., Qiao, M., Chen, D., and Liu, H. **2015**. Single peptide ligand-functionalized uniform hollow mesoporous silica nanoparticles achieving dual-targeting drug delivery to tumor cells and angiogenic blood vessel cells. *Int J Nanomedicine* 10:1855-1867.
- Lu, H., Utama, R. H., Kitiyotsawat, U., Babiuch, K., Jiang, Y., and Stenzel, M. H. **2015**. Enhanced transcellular penetration and drug delivery by crosslinked polymeric micelles into pancreatic multicellular tumor spheroids. *Biomater Sci* 3:1085-1095.
- Marshall, D. R., Lukas, T. J., and Watterson, D. M. **1985**. Drug-protein interactions: binding of chlorpromazine to calmodulin, calmodulin fragments, and related calcium binding proteins. *Biochemistry* 24:144-150.
- Mazard, T., Causse, A., Simony, J., Leconet, W., Vezzio-Vie, N., Torro, A., Jarlier, M., Evrard, A., Del Rio, M., Assenat, E., Martineau, P., Ychou, M., Robert, B., and Gongora, C. **2013**. Sorafenib Overcomes Irinotecan Resistance in Colorectal Cancer by Inhibiting the ABCG2 Drug-Efflux Pump. *Mol Cancer Ther* 12:2121-2134.
- Milani, S., Bombelli, F. B., Pitek, A. S., Dawson, K. A., and Raedler, J. **2012**. Reversible/irreversible Binding of Transferrin to Polystyrene Nanoparticles: Soft and Hard Corona. *ACS Nano* 6:2532-2541.
- Mondal Roy, S., and Sarkar, M. **2011**. Membrane fusion induced by small molecules and ions. *J Lipids* 2011:528784.
- Moody, P. R., Sayers, E. J., Magnusson, J. P., Alexander, C., Borri, P., Watson, P., and Jones, A. T. **2015**. Receptor Crosslinking: A General Method to Trigger Internalization and Lysosomal Targeting of Therapeutic Receptor:Ligand Complexes. *Mol Ther* 23:1888-1898.
- Nacs, J., Nagy, L., Sharples, D., Hever, A., Szabo, D., Ocsosvski, I., Varga, A., Konig, S., and Molnar, J. **1998**. The inhibition of SOS-responses and MDR by phenothiazine-metal complexes. *Anticancer Res* 18:3093-3098.
- Peppas, N. A. **2013**. Historical perspective on advanced drug delivery: How engineering design and mathematical modeling helped the field mature. *Adv Drug Deliv Rev* 65:5-9.
- Quan, G., Pan, X., Wang, Z., Wu, Q., Li, G., Dian, L., Chen, B., and Wu, C. **2015**. Lactosaminated mesoporous silica nanoparticles for asialoglycoprotein receptor targeted anticancer drug delivery. *J Nanobiotechnology* 13:7.



- Rodal, S. K., Skretting, G., Garred, O., Vilhardt, F., van Deurs, B., and Sandvig, K. **1999**. Extraction of Cholesterol with Methyl- $\beta$ -Cyclodextrin Perturbs Formation of Clathrin-coated Endocytic Vesicles. *Mol Biol Cell* 10:961-974.
- Rose, S. D., Cook, H. W., Palmer, F. B. S. C., Ridgway, N. D., and Byers, D. M. **1994**. Differential expression of MARCKS and other calmodulin-binding protein kinase C substrates in cultured neuroblastoma and glioma cells. *J Neurochem* 63:2314-2323.
- Sayers, E. J., Magnusson, J. P., Moody, P. R., Mastrotto, F., Conte, C., Brazzale, C., Borri, P., Caliceti, P., Watson, P., Mantovani, G., Aylott, J. W., Salmaso, S., Jones, A. T., and Alexander, C. **2018**. Switching of Macromolecular Ligand Display by Thermoresponsive Polymers Mediates Endocytosis of Multiconjugate Nanoparticles. *Bioconjug Chem* 29(4):1030-1046.
- Tarasov, A. I., Griffiths, E. J., and Rutter, G. A. **2012**. Regulation of ATP production by mitochondrial  $\text{Ca}^{2+}$ . *Cell Calcium* 52:28-35.
- Tekle, C., van Deurs, B., Sandvig, K., and Iversen, T. G. **2008**. Cellular Trafficking of Quantum Dot-Ligand Bioconjugates and Their Induction of Changes in Normal Routing of Unconjugated Ligands. *Nano Lett* 8:1858-1865.
- Varela, J. A., Bexiga, M. G., Aberg, C., Simpson, J. C., and Dawson, K. A. **2012**. Quantifying size-dependent interactions between fluorescently labeled polystyrene nanoparticles and mammalian cells. *J Nanobiotechnol* 10:39.
- Vercauteren, D., Vandenbroucke, R. E., Jones, A. T., Rejman, J., Demeester, J., De Smedt, S. C., Sanders, N. N., and Braeckmans, K. **2010**. The Use of Inhibitors to Study Endocytic Pathways of Gene Carriers: Optimization and Pitfalls. *Mol Ther* 18:561-569.
- Watson, S. A., Durrant, L. G., and Morris, D. L. **1990**. The effect of the E2 prostaglandin enprostil, and the somatostatin analogue sms 201 995, on the growth of a human gastric cell line, MKN45G. *Int J Cancer* 45:90-94.
- Zan, M., Li, J., Huang, M., Lin, S., Luo, D., Luo, S., and Ge, Z. **2015**. Near-infrared light-triggered drug release nanogels for combined photothermal-chemotherapy of cancer. *Biomater Sci* 3:1147-1156.

## Supporting information

Additional supporting information may be found online in the Supporting Information section at the end of the article.

**Figure S1** Cell Titer Glo toxicity tests of the working concentrations and experimental times of incubations used for 50 and 100 nm C-PS-NPS, CPZ and M $\beta$ CD. The seeding density of cells to obtain a linear relationship between numbers of cells and viability signal was investigated by a titration curve prior to toxicity tests (data not shown). Cells were seeded in 96 well plates at a density of 31200 cells/cm<sup>2</sup> and allowed to attach to the wells overnight. The day after the media was replaced with CPZ 80  $\mu\text{M}$ , M $\beta$ CD 1.25 mM, 50 or 100 nm C-PS-NPS 100  $\mu\text{g}/\text{ml}$  or PEI 500  $\mu\text{g}/\text{ml}$  positive control in HBSS/HEPES 20 mM, and incubated for 4 or 4.5 h. Upon completion of the incubation time, Cell Titer Glo was applied according to standard protocols. Cell Titer Glo toxicity tests were carried out in triplicate

wells in 3 independent experiments. Error bars represent the standard deviation of the mean ( $n = 3$ ).

**Figure 1: Time and cell dependence of HTf uptake inhibition by CPZ (80  $\mu\text{M}$ ) in 3 T3, HCT 116 and MGLVA-1 cells as determined by flow cytometry.** Cells were preincubated with CPZ, M $\beta$ CD or 20 mM HBSS/HEPES for 30 mins. Then, the buffer was aspirated and replaced with 0.81  $\mu\text{M}$  HTf in HBSS/HEPES with or without inhibitors of endocytosis or 20 mM HBSS/HEPES alone and further incubated for 1, 2, 3 or 4 h.

**Figure 2: Concentration and time dependence of HTf uptake inhibition by CPZ in 3 T3 and HCT 116 cells.** Cells were preincubated with HBSS/HEPES 20 mM with or without inhibitor for 30 mins. Subsequently the pre-treatment buffer was aspirated and 3 T3 cells were treated with 40 and 80  $\mu\text{M}$  CPZ for up to 4 h and HCT 116 with 40 and 80  $\mu\text{M}$  of CPZ for up to 4 h.

**Figure 3: Effects of  $\text{Ca}^{2+}$  and  $\text{Mg}^{2+}$  depletion on the uptake of HTf with CPZ in 3 T3 cells.** Cells were pre-incubated with HBSS/HEPES 20 mM devoid of  $\text{Ca}^{2+}$  and  $\text{Mg}^{2+}$  with or without inhibitor for 30 mins. Subsequently the pre-treatment buffer was aspirated and replaced with fresh solutions of HBSS/HEPES 20 mM devoid of  $\text{Ca}^{2+}$  and  $\text{Mg}^{2+}$  with or without HTf 6.7  $\mu\text{g}/\text{ml}$ , different concentrations of CPZ ranging from 40 to 80  $\mu\text{M}$  and 1.25 mM M $\beta$ CD. The cells were further incubated for 1, 2, 3 or 4 h.

**Figure 4: Passage number and ageing of cells affects HTf uptake in the presence of CPZ (80  $\mu\text{M}$ ).** Cells at different passage numbers were incubated with 6.7  $\mu\text{g}/\text{ml}$  HTf and 80  $\mu\text{M}$  CPZ at 1, 2 3 and 4 h in 3 T3 and HCT 116 cells. Graphs show inhibition with 80  $\mu\text{M}$  CPZ in 3 T3 and HCT 116 cells with more than 20 passage numbers difference. Data represent three replicate data points for each experiment for a minimum 2 independent experiments. Cells were treated as in previous experiments with 30 min pre-incubation of CPZ or HBSS/HEPES that was replaced by HBSS/HEPES 20 mM buffer supplemented of HTf for the positive control or 80  $\mu\text{M}$  CPZ and HTf, and further incubated for 1 or 2 h.

**Figure 5: Respective inhibition and stimulation of LacCer uptake by M $\beta$ CD and CPZ.** A pre-incubation step of 30 min was carried out in the presence or absence of endocytosis inhibitors. Upon completion of the pre-incubation time the media was aspirated and replaced with LacCer 0.81  $\mu\text{M}$  in the presence or absence of inhibitors of endocytosis. Cells were incubated for up to 4 h and the results are the combination of 2 independent experiments ( $n = 2$ ), the error bars

represent the standard deviation of the mean from a minimum of 20000 gated cells per experiment.

**Figure 8: Endocytosis of 50 nm and 100 nm C-PS-NPS by cells with and without 80  $\mu$ M CPZ and 1.25 mM M $\beta$ CD.** A pre-incubation step of 30 min was carried out in the presence or absence of endocytosis inhibitors. Upon completion of the pre-incubation time the media were aspirated and replaced with LacCer 0.81  $\mu$ M in the presence or absence of inhibitors of endocytosis. Cells

were incubated for up to 4 h and the results are the combination of 2 independent experiments ( $n = 2$ ). Inhibition of uptake of C-PS-NPS in 3 T3 and HCT 116 cells was monitored for 1 and 2 h while in MGLVA-1 s inhibition of the uptake was examined at 2 and 4 h. The results are shown as the mean and standard deviation of 2 independent flow cytometry experiments obtained on 10000 gated cells ( $n = 2$ ).